Influences of ENSO Teleconnection on the Persistence of Sea Surface Temperature in the Tropical Indian Ocean

RUIQIANG DING AND JIANPING LI

State Key Laboratory of Numerical Modeling for Atmospheric Sciences and Geophysical Fluid Dynamics (LASG), Institute of Atmospheric Physics, Chinese Academy of Sciences, Beijing, China

(Manuscript received 21 December 2011, in final form 3 May 2012)

ABSTRACT

This study confirms a weak spring persistence barrier (SPB) of sea surface temperature anomalies (SSTAs) in the western tropical Indian Ocean (WIO), a strong fall persistence barrier (FPB) in the South China Sea (SCS), and the strongest winter persistence barrier (WPB) in the southeastern tropical Indian Ocean (SEIO). During El Niño events, a less abrupt sign reversal of SSTAs occurs in the WIO during spring, an abrupt reversal occurs in the SCS during fall, and the most abrupt reversal occurs in the SEIO during winter. The sign reversal of SSTA implies a rapid decrease in SSTA persistence, which is favorable for the occurrence of a persistence barrier. The present results indicate that a more abrupt reversal of SSTA sign generally corresponds to a more prominent persistence barrier. El Niño–induced changes in atmospheric circulation result in reduced evaporation and suppressed convection. This in turn leads to the warming over much of the TIO basin, which is an important mechanism for the abrupt switch in SSTA, from negative to positive, in the northern SCS and SEIO. The seasonal cycle of the prevailing surface winds has a strong influence on the timing of the persistence barriers in the TIO.

The Indian Ocean dipole (IOD) alone can cause a weak WPB in the SEIO. El Niño events co-occurring with positive IOD further strengthen the SEIO WPB. The SEIO WPB appears to be more strongly influenced by ENSO than by the IOD. In contrast, the WIO SPB and the SCS FPB are relatively independent of the IOD.

1. Introduction

El Niño–Southern Oscillation (ENSO) is the dominant mode of variability in the tropical Pacific at interannual time scales and has a widespread effect on the global climate system. During El Niño, a sea surface temperature anomaly (SSTA) in the equatorial eastern Pacific develops during summer, peaks during winter, and decays in the following spring. El Niño is normally accompanied by a shift in atmospheric convection from the western to the eastern tropical Pacific. By shifting tropical convection, El Niño forces a delayed (relative to the mature phase of El Niño) spring warming of the tropical Indian Ocean (TIO) (Klein et al. 1999; Alexander et al. 2002; Lau and Nath 2003) and of the northern tropical Atlantic (NTA) (Enfield 1996; Enfield and Mayer 1997) via atmospheric teleconnection. Herein, the seasons refer to those for the Northern Hemisphere. The TIO includes the tropical Indian Ocean basin as well as the South China Sea (SCS) and Indonesian Seas.

Because of a large SSTA and a strong atmospheric bridge effect in the tropics, the El Niño–forced warming of the TIO and NTA can persist from spring to summer, strongly influencing the spring and summer regional climate. For example, the NTA warming forces a northward displacement of the Atlantic intertropical convergence zone (ITCZ), resulting in increased precipitation over the Caribbean and reduced precipitation over northeast Brazil during spring following the mature phase of El Niño (Nobre and Shukla 1996; Giannini et al. 2001). The TIO warming, following El Niño, has a strong influence on the summer climate over the Indo–western Pacific and East Asia, leading to an anomalous anticyclone over the subtropical northwest Pacific and increased mei-yu–baiu rainfall over East Asia (Ding et al. 2009; Xie et al. 2009). In this way, the persistent SSTA in the TIO and NTA plays an important role in passing the ENSO information in winter to the regional climate of the following

Corresponding author address: Dr. Jianping Li, State Key Laboratory of Numerical Modeling for Atmospheric Sciences and Geophysical Fluid Dynamics (LASG), Institute of Atmospheric Physics, Chinese Academy of Sciences, P.O. Box 9804, Beijing 100029, China.
E-mail: ljp@lasg.iap.ac.cn

DOI: 10.1175/JCLI-D-11-00739.1

spring and summer. Consequently, a better understanding of the persistence characteristics of the TIO and NTA SSTA associated with ENSO should benefit climate predictions for East Asia and the tropical Atlantic.

In the tropical central–eastern Pacific, Webster and Yang (1992) found that autocorrelations of ENSO anomalies show a rapid and significant decrease in the spring months of March–May, which is known as the phenomenon of the spring persistence barrier (SPB). Considerable research effort has been devoted to investigating the SPB in ENSO anomalies because of its great influence on ENSO prediction (e.g., Zebiak and Cane 1987; Goswami and Shukla 1991; Torrence and Webster 1998; Clarke and Van Gorder 1999; Yu 2005; Duan et al. 2009). In addition to the well-known SPB in the Pacific, several previous studies have found that associated with ENSO, the persistence barrier of the SSTA also occurs in the TIO and NTA during seasons other than summer. Nicholls (1984) reported that the Indonesian SSTA shows strong persistence from January to October, with a tendency to dissipate around November, a phenomenon now referred to the winter persistence barrier (WPB). His analysis demonstrated that changes in the Indonesian SSTA persistence are closely related to ENSO phenomena. Wajsowicz (2005) and Luo et al. (2007) reported a SPB of the SSTA in the western TIO (WIO), related to ENSO influences. Chen et al. (2007) reported a fall persistence barrier (FPB) of the SSTA in the SCS, and Ding and Li (2011) reported a WPB of the SSTA in the NTA. Both the SCS and NTA barriers are prominent during strong ENSO events but become indistinct during weak ENSO and normal (i.e., non-ENSO) events. During strong ENSO events, the SCS SSTA shows a reversal in sign during fall, whereas the NTA SSTA shows a reversal in sign during winter. Chen et al. (2007) and Ding and Li (2011) concluded that the SSTA sign reversal in the SCS and NTA during strong ENSO events results in reduced persistence, possibly leading to the occurrence of the SCS and NTA barriers. These barriers, which are similar to the ENSO SPB, may significantly affect the skill of SST predictions when predictions are made across seasons in which the barriers occur.

In addition to ENSO, the other major mode of interannual variability that impacts the Indian Ocean (IO) is the Indian Ocean dipole (IOD; also called the Indian Ocean zonal mode) (Saji et al. 1999). The positive IOD event is characterized by a positive SSTA in the WIO and a negative SSTA in the southeastern TIO (SEIO). Similarly to ENSO, the IOD is characterized by strong seasonal phase locking; it develops during summer, reaches a peak in fall, and decays in winter. The seasonal phase locking of the IOD event has an important influence on the persistence of the TIO SSTA. Wajsowicz (2005) reported a WPB of the SSTA in the SEIO, and concluded that the SEIO WPB may be caused by strong seasonal phase locking of the IOD. According to Saji et al. (1999), some positive (negative) IOD events, but not all, occur during the same year as El Niño (La Niña). Given that IOD often co-occurs with ENSO, it is very likely that both ENSO and IOD affect the WPB in the SEIO. Previous studies (e.g., Chowdary and Gnanaseelan 2007; Hong et al. 2010) have investigated the relative contribution of ENSO and IOD to the rapid warming in SEIO. However, a detailed analysis of the relative contributions of ENSO and IOD to the SEIO barrier is still lacking. Nicholls (1984) and Wajsowicz (2005) only investigated the role of ENSO and IOD alone, respectively, in inducing the SEIO WPB.

In our previous paper (Ding and Li 2011), we performed a detailed analysis of the persistence of the NTA SSTA for different ENSO cases. The present paper reports on the persistence characteristics of the TIO SSTA. In addition to establishing the existence of the ENSO-induced WIO SPB and SCS FPB, we consider the following questions regarding the persistence of the TIO SSTA: Does the remote influence of ENSO also lead to a WPB in the SEIO? If so, what are the relative contributions of ENSO and IOD to the occurrence of the SEIO WPB? Why does the WIO barrier occur in spring and the SCS barrier in fall, when the SEIO barrier occurs in winter? Do the WIO, SCS, and SEIO barriers differ in intensity? The purpose of the present study is to answer these questions.

The remainder of this paper is organized as follows. Section 2 describes the data and analysis methods. Section 3 analyzes the evolution of the TIO SSTA associated with ENSO. Section 4 investigates the persistence of the SSTA in various TIO subdomains. Section 5 explores the mechanisms by which ENSO affects the evolution of the TIO SSTA. Section 6 investigates the relative contributions of ENSO and IOD to the persistence of the TIO SSTA. Finally, a summary is presented in section 7.

2. Data and methodology

This study employs the Hadley Center Sea Ice and SST dataset (HadISST) on a $1° \times 1°$ spatial grid for the period 1900–2007 (Rayner et al. 2006), and the National Centers for Environmental Prediction–National Center for Atmospheric Research (NCEP–NCAR) atmospheric reanalysis on a $2.5° \times 2.5°$ grid for 1950–2007 (Kalnay et al. 1996). The NCEP–NCAR reanalysis includes wind, streamfunction, and surface heat flux fields.

The present study focuses on interannual variability associated with ENSO. To reduce the effect of pronounced decadal variability over the Indian Ocean (Ashok et al. 2004; Alory et al. 2007), the climatological mean annual cycle is removed, leaving the anomalies, which are then

TABLE 1. Member years of strong ENSO, weak ENSO, and normal (non-ENSO) cases for the period 1950–2007.

Strong ENSO	El Niño	1957, 1965, 1972, 1982, 1986, 1987, 1991, 1994, 1997, 2002
	La Niña	1954, 1955, 1964, 1970, 1973, 1975, 1988, 1998, 1999, 2007
Weak ENSO	El Niño	1951, 1963, 1968, 1969, 1976, 1977, 2004, 2006
	La Niña	1950, 1956, 1962, 1967, 1971, 1974, 1984, 1995, 2000
Normal	Positive	1952, 1953, 1958, 1979, 1990, 1992, 1993, 2003
	Negative	1959, 1960, 1961, 1966, 1978, 1980, 1981, 1983, 1985, 1989, 1996, 2001, 2005

passed through a 7-yr high-pass Gaussian filter. In this way, the annual cycle and decadal components are removed from the monthly data, while leaving the anomalies. Autocorrelation analysis was used to measure the persistence of the SSTA, which is defined as the correlation between the time series of the starting calendar month (January–December) and the time series of a succeeding lag month over a period of given duration (Ding and Li 2009, 2011).

We use the area-averaged SST over the Niño-3 region (5°S–5°N, 150°–90°W) as the ENSO index. To investigate the relationship between ENSO and TIO SSTA persistence, ENSO cases were classified into three types according to the intensity of the Niño-3 SST index at its peak phase: November(0)–January(1) [NDJ(0)] for the period 1950–2007. Here, the numerals ''0'' and ''1'' denote the developing year and the decay year of ENSO, respectively. A strong (weak, normal) ENSO case is defined as a year in which the Niño-3 SSTA at its peak phase has an intensity greater than 1.0 (0.5–1.0, <0.5) SD of its 1950−2007 time series (Table 1).

To investigate the relative effects of ENSO and IOD on the persistence of the TIO SSTA, all years in the period 1900–2007 are classified as positive or negative IOD, El Niño or La Niña, or neutral years (Table 2). The classification is based mainly on Meyers et al. (2007) but adjusted according to ENSO and IOD indices at their respective mature phases [September–November (SON) for IOD]. The IOD index is defined as SSTA differences between the WIO (10°S–10°N, 50°–70°E) and the SEIO (10°S–0°, 90°–110°E) (Saji et al. 1999). After adjustment, strong ENSO or IOD years are maintained as ENSO or IOD years, but weak ENSO or IOD years are reclassified as non-ENSO or non-IOD years. In Table 2, El Niño and La Niña years after 1950 are equivalent to the strong El Niño and La Niña years shown in Table 1.

3. Evolution of the TIO SSTA associated with ENSO

Previous studies have noted that while El Niño–induced warming ultimately covers the entire TIO basin, the TIO warming often shows significant variations in space and time (Kawamura et al. 2001; Schott et al. 2009). In this section, we examine in detail the evolutionary features of the ENSO-induced TIO SSTA, with the aim of identifying the possible influence of these features on the SSTA persistence.

Figure 1 shows composite difference patterns of the SSTA (strong El Niño minus strong La Niña) during the developing and mature phases of ENSO [August(0) to March(1)]. The central and eastern equatorial Pacific is dominated by strong and sustained warming, accompanied by a minor cooling in the tropical western Pacific, which reflects the typical features of El Niño evolution. The maximum warming occurs in the eastern equatorial Pacific during December(0) and January(1), indicating that El Niño reaches its mature phase. After February(1), El Niño enters its decaying stage. As a delayed response to El Niño, the TIO warming shows distinct regional

TABLE 2. Classification of years in which El Niño or La Niña and/or positive or negative IOD occurred during the period 1900–2007.

	Negative IOD	No event	Positive IOD
El Niño	1930	1905, 1911, 1914, 1918, 1925, 1940, 1941, 1965, 1986, 1987, 2002	1902, 1957, 1972, 1982, 1991, 1994, 1997
No event	1917, 1928, 1958, 1968, 1974, 1980, 1985, 1989, 1992, 1996, 2005	1900, 1901, 1904, 1907, 1908, 1910, 1912, 1915, 1920, 1921, 1927, 1929, 1931, 1932, 1934, 1936, 1937, 1939, 1943, 1945, 1947, 1948, 1950, 1951, 1952, 1953, 1956, 1959, 1960, 1962, 1966, 1969, 1971, 1976, 1977, 1979, 1981, 1983, 1984, 1990, 1993, 1995, 2000, 2001, 2003	1913, 1919, 1923, 1926, 1935, 1944, 1946, 1961, 1963, 1967, 1978, 2004, 2006
La Niña	1906, 1909, 1916, 1933, 1942, 1975, 1988	1903, 1922, 1924, 1938, 1949, 1954, 1955, 1964, 1970, 1973, 1998, 1999, 2007	

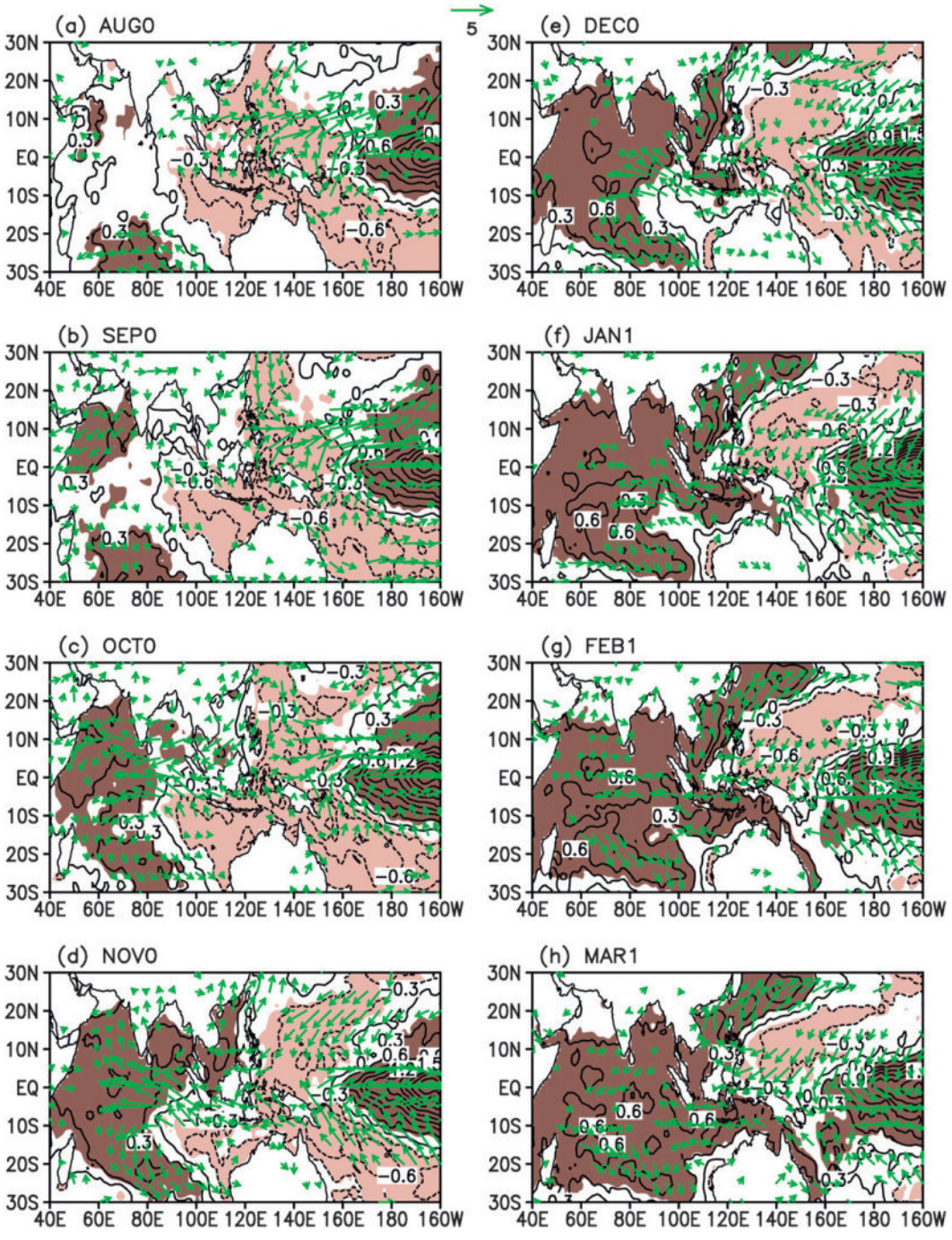

FIG. 1. Composite difference of the SSTA (°C; contours) and surface wind velocity (m s^{-1}; vectors) for strong ENSO cases (El Niño − La Niña) during their developing and mature phases [August(0) to March(1)]. The contour interval of the SSTA is 0.3°C; positive (dark brown) and negative (light brown) SSTAs, significant at the 95% level, are shaded. Only wind vectors significant at the 95% level are shown.

characteristics. The TIO warming first takes place in the southern IO (SIO) (30°–20°S, 60°–90°E) in August(0). An anomalous warming in the Arabian Sea begins to emerge in September(0) and extends southward and eastward to cover the entire WIO and northern IO (NIO; including the SCS) in November(0). After December(0), the TIO warming begins to stretch farther southeastward into the SEIO. Basinwide warming over the TIO

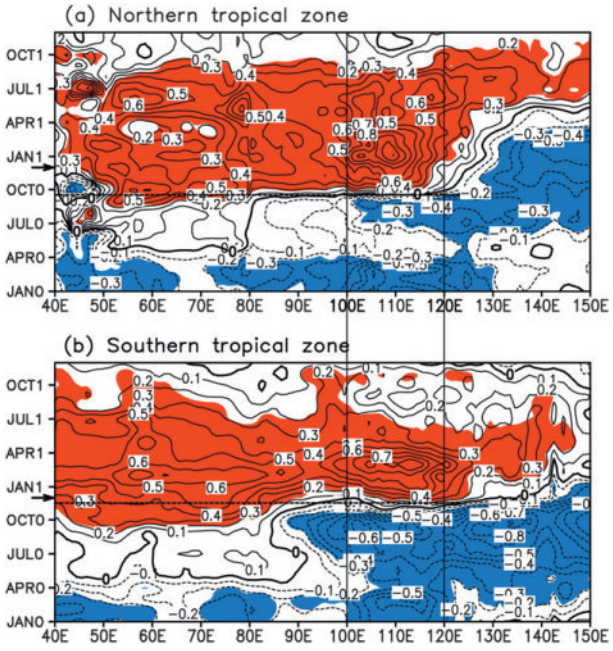

FIG. 2. Longitude–time diagrams of the composite difference of the SSTA averaged over (a) the 5°–20°N zone and (b) the 15°S–0° zone for strong ENSO cases (El Niño − La Niña). The contour interval is 0.1°C; positive (red) and negative (blue) anomalies of the SSTA, significant at the 95% level, are shaded. The horizontal black arrow denotes December(0), the peak phase of ENSO; the 100°–120°E zone is bounded by two vertical lines; the horizontal dashed line indicates the approximate occurrence time of the abrupt reversal in SSTA sign.

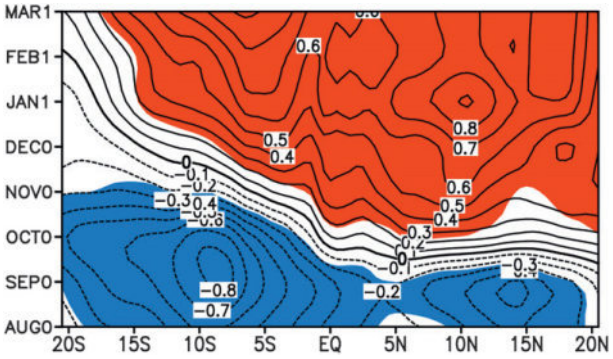

FIG. 3. Latitude–time diagram of the composite difference of the SSTA averaged over the 100°–120°E zone for strong ENSO cases (El Niño − La Niña). The contour interval is 0.1°C; positive (red) and negative (blue) anomalies of the SSTA, significant at the 95% level, are shaded.

appears in February(1) and is maintained through the ensuing spring. Overall, these features are consistent with the results of previous observational and modeling studies (Klein et al. 1999; Venzke et al. 2000; Alexander et al. 2002; Lau and Nath 2003).

Figure 1 shows that the warming in the SCS and SEIO is more abrupt than the warming elsewhere. The SCS is dominated by anomalous cooling during August(0) and September(0), and anomalous warming emerges in the southern SCS in October(0), extending northward to cover the entire SCS in December(0) with a maximum warming center located to the east of Taiwan, consistent with the results of Chen et al. (2007). Compared with the SCS, the cooling is more intense in the SEIO off the west coast of Sumatra and Java, and it persists from August(0) to November(0), interrupted by an anomalous warming after December(0). These results suggest that the SCS and SEIO SSTAs, influenced by ENSO, undergo a rapid sign reversal from negative to positive during September–October(0) and November–December(0), respectively.

Figure 2a shows a longitude–time diagram of the composite difference of the SSTA (strong El Niño minus strong La Niña) averaged over the zone from 5°N to 20°N. Figure 2b is the same as Fig. 2a, but for the composite difference of the SSTA averaged from 15°S to the equator. These figures show a rapid change in the SSTA, with the sign changing from negative to positive, mainly in the 100°–120°E zone of the northern and southern tropics (corresponding to longitude ranges of the SCS and SEIO, respectively). The rapid SSTA change in the SCS occurs in fall, one season earlier than the rapid change in the SEIO. For the WIO in the 50°–80°E zone, a very weak positive SSTA occurs in early summer and then persists for several months, finally becoming significant in October(0). In comparison, the SSTA sign reversal from negative to positive is less abrupt in the WIO than in the SCS and SEIO.

To clearly show meridional differences in the evolution of ENSO-related SSTA along the 100°–120°E zone, Fig. 3 shows a latitude–time diagram of the composite difference in the SSTA averaged over the zone from 100° to 120°E. A rapid change in SSTA sign occurs almost simultaneously during September–October(0) at all latitudes from 5° to 20°N (corresponding to the latitude range of the SCS). However, the SSTA in the 15°S–0° zone (corresponding to the latitude range of the SEIO) evolves in a different way; that is, the transition in SSTA sign is progressively delayed with increasing latitude from the equator to 15°S, occurring at the equator around October(0), one month earlier than the transition at 10°S. The zonal average of the SSTA along the 15°S–0° zone shows a phase transition at some point during November(0) or December(0), as shown in Fig. 2b.

Based on the evolutionary features of the ENSO-related TIO SSTA, we focus on three regions: the WIO (10°S–10°N, 50°–70°E), SCS (5°–20°N, 100°–120°E), and SEIO (15°S–0°, 100°–120°E). Figure 4 shows the detailed evolutions of ENSO itself and ENSO-related SSTA averaged over the WIO, SCS, and SEIO, as represented

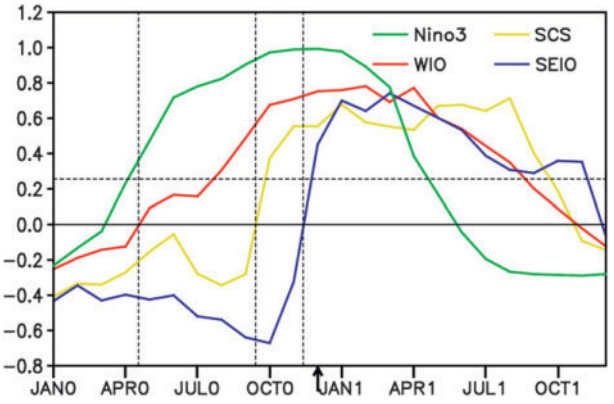

FIG. 4. Correlation of the November(0)–January(1) [NDJ(0)] Niño-3 SST index with SST averaged over the WIO (10°S–10°N, 50°–70°E), SCS (5°–20°N, 100°–120°E), and SEIO (15°S–0°, 100°–120°E). The green line shows the lagged autocorrelation of the Niño-3 SST index with its NDJ(0) values. The horizontal dashed line indicates the 95% significance level. The vertical black arrow denotes December(0), the peak phase of ENSO.

by their correlations with the Niño-3 SST index at its peak phase [NDJ(0)]. Significant ENSO-related warming (≥0.26°C) occurs gradually over the WIO, SCS, and SEIO, with a lag of 1–2 months. The WIO SSTA shows a sign reversal from negative to positive during April–May(0), whereas the SCS and SEIO SSTA show a sign reversal from negative to positive during September–October(0) and November–December(0), respectively. The WIO warming becomes significant in fall and peaks in February(1). It takes 3–4 months for the minor positive SSTA in the WIO to become significant. In contrast, it takes only one month for the minor positive SSTA in the SCS and SEIO to become significant. These results confirm that the warming is more abrupt in the SCS and SEIO than in the WIO. The SEIO warming reaches a maximum around March(1), about one season after the peak in the Niño-3 SSTA. The SCS warming shows two peaks: one in January(1) and the other in August(1), consistent with the findings of Du et al. (2009). The second warming peak in the SCS (also in the NIO) leads to a long persistence of the TIO warming induced by El Niño, exerting a profound influence on summer climate around East Asia (Du et al. 2009; Xie et al. 2009).

As expected, the TIO warming during weak El Niño events is not as strong as that during strong El Niño events (Fig. 5). The same is true of the cooling that occurs prior to the warming in the 100°–120°E zone. Therefore, the sign reversal of SSTA in the SCS and SEIO becomes indistinct during weak El Niño events. For normal ENSO cases, the amplitude of the TIO SSTA is very small and the evolution of the TIO SSTA is relatively chaotic (not shown). The sign reversal of SSTA in the SCS and SEIO does not occur during normal ENSO cases.

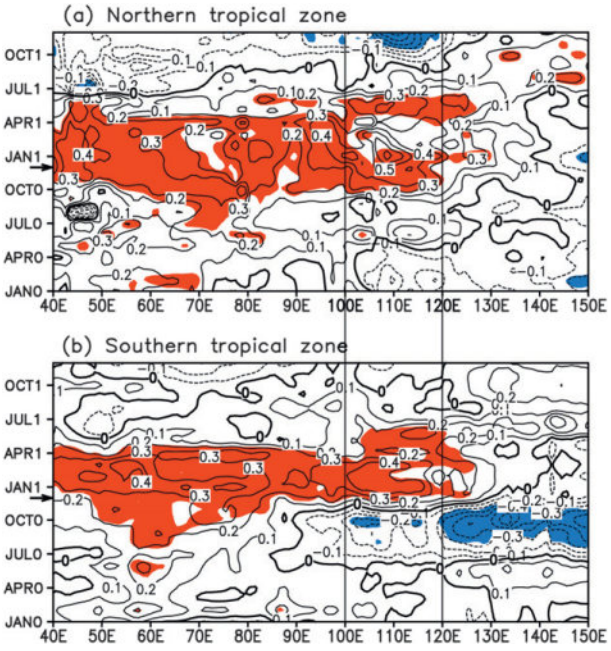

FIG. 5. As in Fig. 2, but for longitude–time diagrams of the composite difference of the SSTA averaged over (a) the 5°–20°N zone and (b) the 15°S–0° zone for weak ENSO cases (El Niño − La Niña).

4. Persistence characteristics of the SSTA in various TIO subdomains

The ENSO-induced SSTA in the WIO, SCS, and SEIO show contrasting evolutionary features; however, it is unclear how these features affect the persistence of SSTA in the three TIO subdomains. This section examines the persistence characteristics of SSTA in the WIO, SCS, and SEIO, respectively.

a. Persistence characteristics over the entire period (1950–2007)

The left panels in Fig. 6 show the autocorrelations of the area-averaged SSTA over the WIO, SCS, and SEIO for the period 1950–2007. The right panels contain the same information as the left panels, but clearly show the occurrence time of a persistence barrier. Autocorrelations significant at the 95% level (≥0.26) are shaded in the left panels. The time taken for autocorrelation to drop below the 95% significance level can be regarded as a measure of SST persistence starting from that month.

Figure 6a shows that the WIO SSTA has a high persistence in the starting months from August(0) to October(0) (autocorrelations fall below the 95% significance level after about 6 months). The persistence of the WIO SSTA shows a slow rise from March(0) to September(0), and a slow decline from January(0) to March(0). These results demonstrate that the WIO SSTA has a minimum

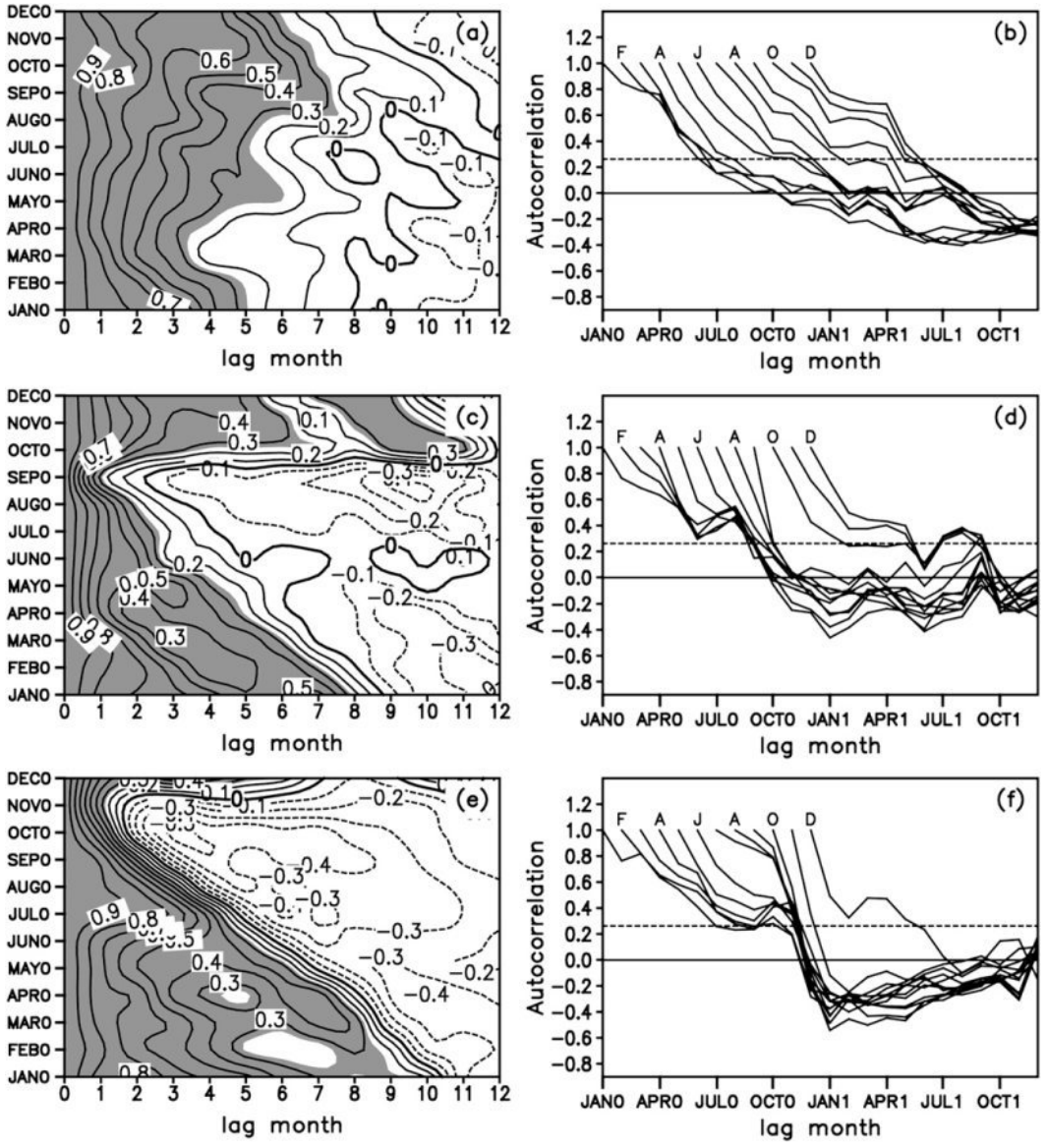

FIG. 6. (left) Autocorrelations of the area-averaged SSTA over the (a) WIO, (c) SCS, and (e) SEIO as a function of starting calendar month and lag time for the period 1950–2007. (right) Autocorrelation curves of the (b) WIO, (d) SCS, and (f) SEIO SSTA as a function of starting calendar month and lag time. In (a),(c), and (e), the zero contour is highlighted; autocorrelations significant at the 95% level ($\geq$0.26) are shaded. In (b),(d), and (f), each curve has been shifted to line up the starting month (shown at the top, where FAJAOD = February, April, June, August, October, December) with the corresponding lag month (x axis); the horizontal dashed line indicates the 95% significance level.

persistence in spring [March–April(0)]. From Fig. 6b, autocorrelations of the WIO SSTA show a relatively rapid decrease in April–May(0), regardless of the starting month. The persistence of the WIO SSTA seems to encounter a barrier in spring [April–May(0)]. According to Webster and Yang (1992), the persistence barrier refers to a phenomenon of autocorrelations showing a rapid and significant decrease (the autocorrelation is reduced to half its value) from one month to the next, regardless of the starting month. However, the autocorrelation value of the WIO SSTA in April(0) is more than half of that in May(0) for most of the starting months. According to Webster and Yang (1992)'s criterion, a robust SPB does not occur in the WIO; instead, it is only weakly developed.

Autocorrelations of the SCS SSTA show a rapid decrease in October–November(0), regardless of the starting month (Fig. 6d). This rapid decrease leads to a minimum

persistence in September(0) (Fig. 6c). The persistence of the SCS SSTA shows a continuous drop before September(0), and a sharp rise thereafter. It therefore appears that the persistence of the SCS SSTA encounters a major barrier in fall [October–November(0)]. An examination of autocorrelations of the SCS SSTA reveals that autocorrelation in October(0) is about half or less of that in November(0) for most of the starting months. This result indicates a prominent FPB in the SCS. In contrast to the SCS SSTA, the persistence of the SEIO SSTA shows a stronger seasonal dependence. Autocorrelations of the SEIO SSTA show a sharp drop in December(0) –January(1), regardless of the starting month (Fig. 6f). This rapid drop in autocorrelations in the SEIO during December(0) –January(1) is more significant than that in the SCS during October–November(0). The most prominent WPB occurs in the SEIO.

b. *Relationship between ENSO and TIO barriers*

To examine the dependence of the WIO SPB, SCS FPB, and SEIO WPB on ENSO, ENSO cases are classified into three types based on the intensity of the Niño-3 SST index at its peak phase: strong, weak, and normal. For strong ENSO cases, the WIO SSTA shows a minimum persistence around March(0) (Fig. 7a), while the SCS and SEIO SSTA show a minimum persistence around September(0) and November(0), respectively (Figs. 7c,e). Autocorrelations of the WIO SSTA starting from January(0) to March(0) show a rapid decrease in April–May(0) (Fig. 7b). Autocorrelations of the SCS SSTA starting from January(0) to September(0) fall quickly below the significance level in October–November(0) (Fig. 7d). Autocorrelations of the SEIO SSTA starting from January(0) to November(0) fall quickly from a large positive correlation to a large negative correlation in December(0)–January(1) (Fig. 7f). These persistence characteristics of the WIO, SCS, and SEIO SSTA for strong ENSO cases are similar to those for the entire period, as shown in Fig. 6. Clearly, there exists a less robust SPB in the WIO, a robust FPB in the SCS, and the most robust WPB in the SEIO during the developing year of strong ENSO cases.

For weak ENSO cases, autocorrelations of the WIO SSTA starting from January(0) to March(0) show a rapid decrease in May(0), associated with a minimum persistence in April(0) (Figs. 8a,b). This rapid decrease of autocorrelations in May(0) during weak ENSO cases is similar to, but slightly less significant than, that during strong ENSO cases. Therefore, the SPB in the WIO SSTA becomes more indistinct during weak ENSO cases. For normal ENSO cases, autocorrelations of the WIO SSTA starting from January(0) to March(0) show a slow decrease in April–May(0), and the minimum persistence does not occur in March(0) or April(0) (not shown). The SPB of the WIO SSTA is absent in normal ENSO cases.

For weak ENSO (Fig. 8) and normal cases (not shown), autocorrelations of the SCS and SEIO SSTA evolve differently from those during strong ENSO cases, and do not show a rapid decrease during fall or winter. The FPB of the SCS SSTA and the WPB of the SEIO SSTA become indiscernible, or do not occur at all, in these two cases.

c. *Mechanisms of barrier development*

The above results confirm the existence of the SEIO SPB, SCS FPB, and SEIO WPB, which have been noted in previous studies (Wajsowicz 2005; Chen et al. 2007; Luo et al. 2007; Zhao and Li 2009). What causes the persistence barriers of the WIO, SCS, and SEIO SSTA during strong ENSO cases? In section 3, we showed that during strong El Niño cases, the sign reversal of SSTA, from negative to positive, occurs successively in the WIO during spring, in the SCS during fall, and in the SEIO during winter, consistent with the seasons during which the persistence barriers occur. Moreover, a slow reversal of SSTA sign in the WIO corresponds to a weak WIO barrier, while an abrupt reversal in the SCS corresponds to a strong SCS barrier, and the most abrupt reversal in the SEIO corresponds to the strongest SEIO barrier. The occurrence seasons and strengths of the persistence barriers are consistent with those of the SSTA sign reversal, indicating a close connection between the two phenomena. The sign reversal of SSTA implies a rapid decrease in the SSTA persistence, which is favorable for the occurrence of a persistence barrier. A more abrupt reversal of SSTA sign should lead to a more prominent persistence barrier. Consequently, the WIO SSTA tends to have a weak persistence barrier in spring, while the SCS SSTA has a strong persistence barrier in fall and the SEIO SSTA has the strongest persistence barrier in winter.

5. Mechanisms by which ENSO affects the evolution of the TIO SSTA

The mechanisms by which El Niño induces a basin-wide warming in the TIO have been extensively studied (e.g., Klein et al. 1999; Alexander et al. 2002; Xie et al. 2002; Lau and Nath 2003; Shinoda et al. 2004; Tokinaga and Tanimoto 2004). However, previous studies focused on the causes of significant warming in the TIO, whereas few studies have examined how ENSO causes a rapid sign reversal in the WIO, SCS, and SEIO SSTA, despite the fact that such an investigation is necessary to identify the mechanisms that induce the persistence barriers. In this section, we investigate in detail how ENSO causes successive sign reversals in the WIO, SCS, and SEIO SSTA.

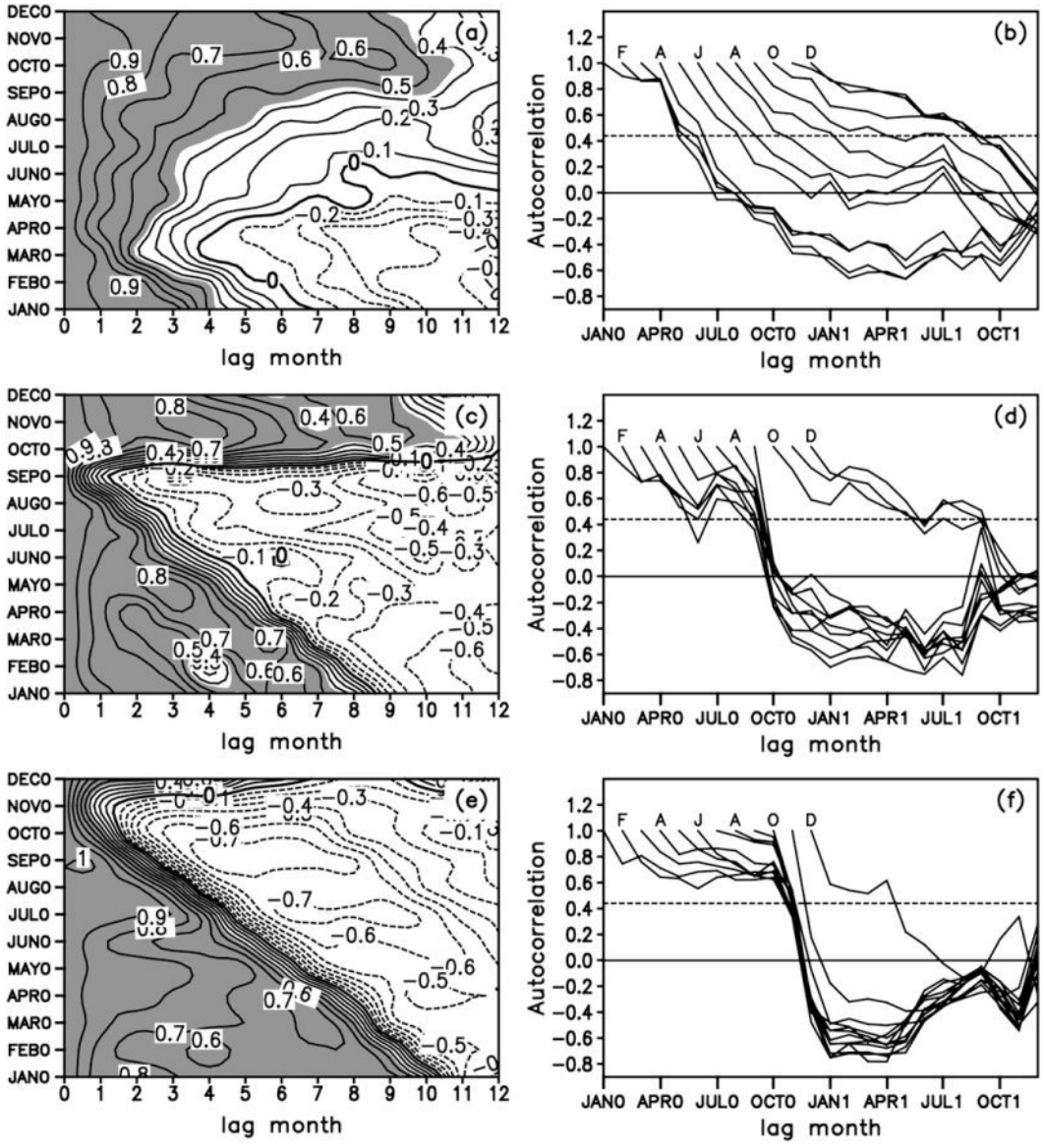

FIG. 7. (left) Autocorrelations of the area-averaged SSTA over the (a) WIO, (c) SCS, and (e) SEIO as a function of starting calendar month and lag time for strong ENSO cases. (right) Autocorrelation curves of the (b) WIO, (d) SCS, and (f) SEIO SSTA as a function of starting calendar month and lag time for strong ENSO cases. In (a),(c), and (e), the zero contour is highlighted; autocorrelations significant at the 95% level are shaded. In (b),(d), and (f), the starting months are in year (0) (i.e., prior to the winter mature phase of ENSO); the horizontal dashed line indicates the 95% significance level.

The quasi-biennial component of ENSO variability has been noted previously (Rasmusson et al. 1990). El Niño events are often preceded or followed by La Niña events. In Fig. 2, the negative SSTA in the TIO that exists before spring could be caused by La Niña events preceded by strong El Niño events. As a La Niña event enters its decaying phase in spring, the negative SSTA in the WIO gradually changes to positive, while the negative SSTA is sustained in the SEIO and SCS. In September(0), a pair of low-level anticyclonic streamfunction anomalies can be clearly observed on each side of the equator, with their centers located around the Arabian Sea and the southwestern TIO (SWIO) (Fig. 9). The two anticyclonic anomalies are caused by the anomalous heat sink over the Maritime Continent (the sinking branch of the anomalous Walker circulation), which forces descending Rossby waves to the west of the Maritime Continent (Gill 1980; Wang and Zhang 2002).

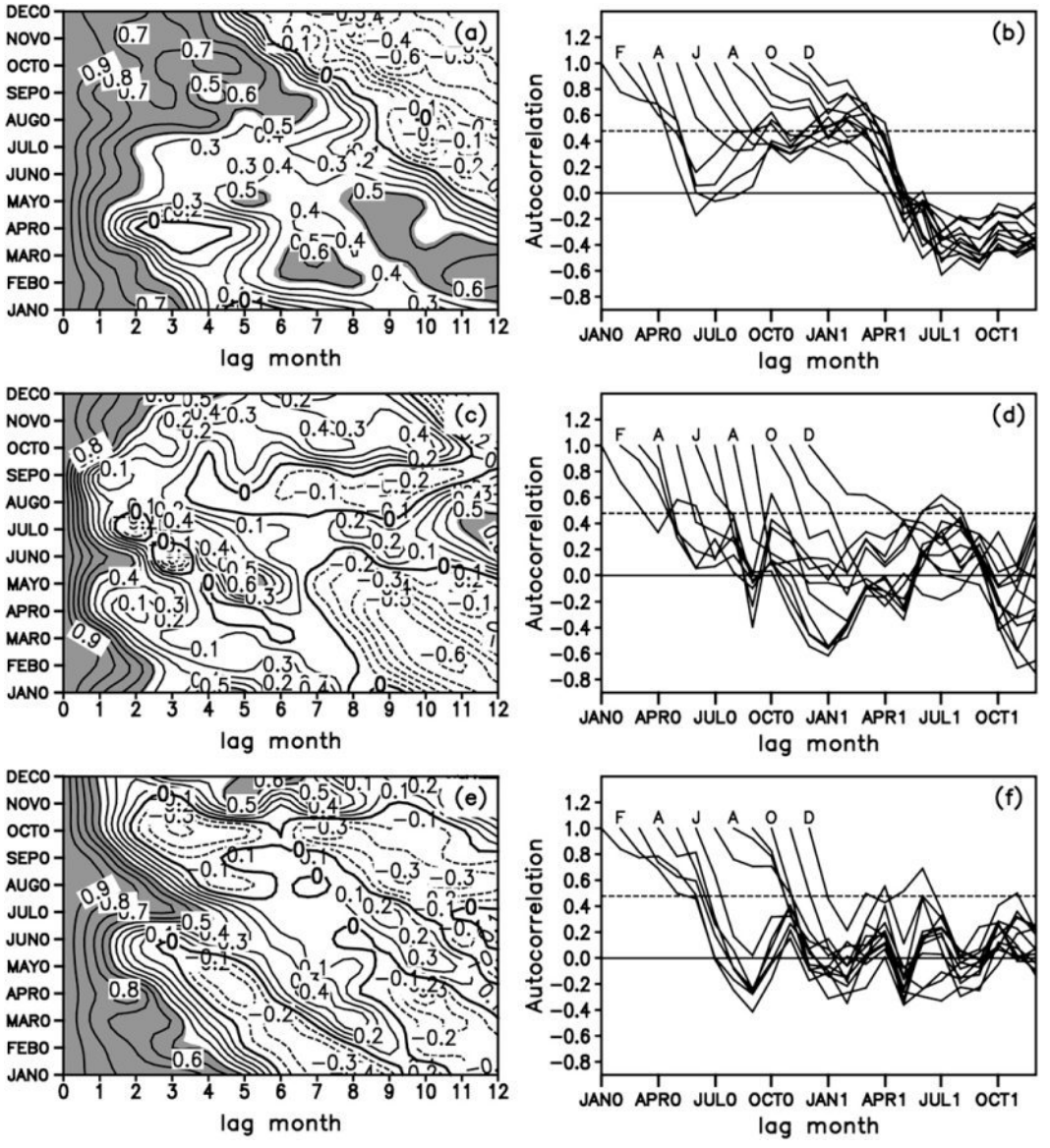

FIG. 8. As in Fig. 7, but for (left) the autocorrelations of the area-averaged SSTA over the (a) WIO, (c) SCS, and (e) SEIO and (right) the autocorrelation curves of the (b) WIO, (d) SCS and (f) SEIO SSTA for weak ENSO cases.

The two anticyclonic anomalies induce an antisymmetric wind pattern that weakens the prevailing southwesterlies and results in an enhanced SSTA in the Arabian Sea in September(0) (Fig. 1). They intensify rapidly and move eastward in October(0) and November(0). The northern edge of the anomalies moves farther eastward into the western North Pacific, with the center over the Philippines in December(0). It eventually anchors in the SCS–Philippines region in the following January(1) and February(1), which is referred to as the anomalous Philippine Sea anticyclone (PSAC) (Wang et al. 2000; Wang and Zhang 2002). Chen et al. (2007) attributed the SCS warming initiated in October(0) to the rapid passage of the northern low-level anomalous anticyclone (NLAAC) during strong El Niño cases. They noted that the SCS is dominated by persistent low-level cyclonic anomalies before September(0) that are associated with an anomalous cooling in the region. The eastward passage of the NLAAC across the SCS, which acts to weaken the prevailing northeasterlies and suppress convection in the SCS, induces changes in surface heat fluxes that in turn generate an anomalously warm SST in the region.

However, our analyses suggest a different cause of SCS warming. The significant warming in the northern SCS (NSCS) (15°–25°N) after November(0) during El Niño cases arises mainly from decreased latent heat flux

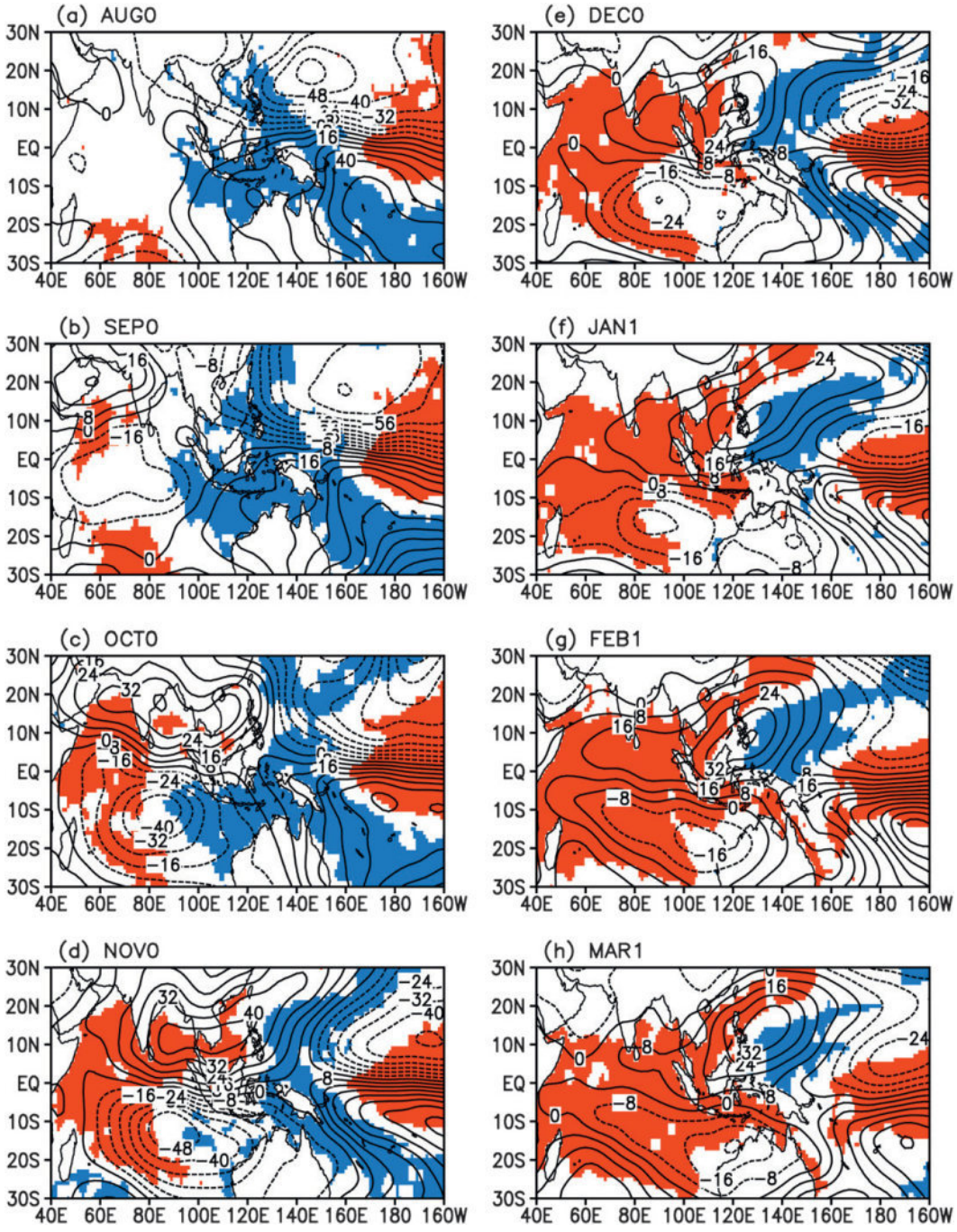

FIG. 9. Composite difference anomalies of the 850-mb level streamfunction (contours) and the SSTA (shaded) for strong ENSO cases (El Niño − La Niña) during the developing and mature phases [August(0) to March(1)]. Contour intervals of streamfunction are 8×10^5 m^2 s^{-1}; positive (red) and negative (blue) anomalies of the SSTA, significant at the 95% level, are shaded.

(LF) loss from ocean to atmosphere, as well as enhanced net shortwave (SW) downward radiation (Fig. 10), which is consistent with the findings of Chen et al. (2007). However, the NLAAC produces easterly wind anomalies in the southern SCS (SSCS) (5°–15°N) after October(0) (Fig. 1), which tends to intensify (not weaken) the prevailing northeasterlies in this region. The LF loss from ocean to atmosphere in the SSCS shows a significant increase after October(0). The minor SW increase due to suppressed convection by the NLAAC cannot compensate

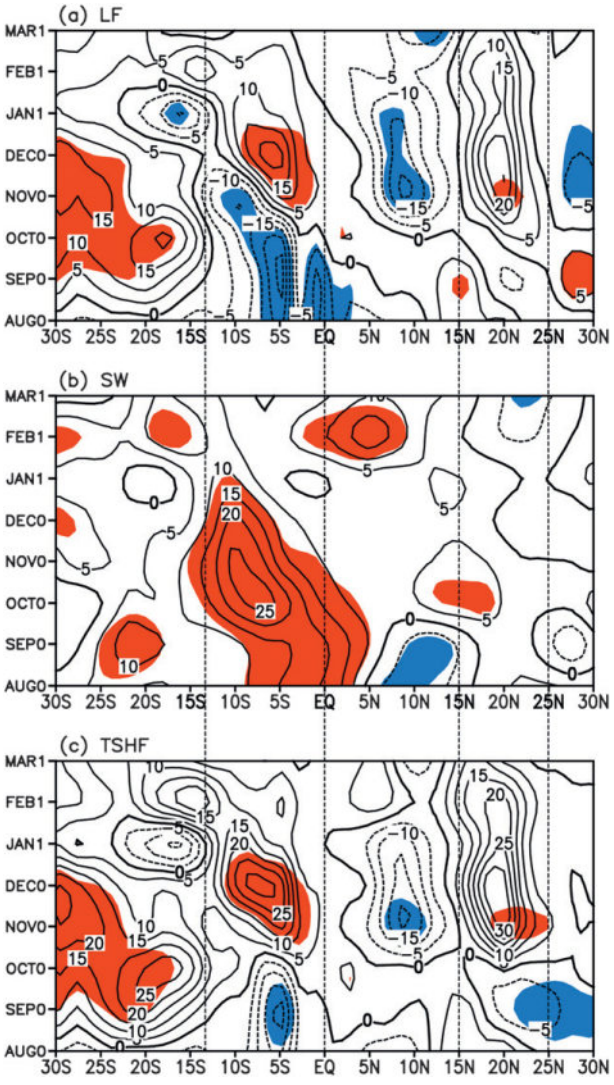

FIG. 10. Latitude–time diagrams of the composite difference of the (a) latent heat flux (LF), (b) net downward shortwave (SW) radiation, and (c) total surface heat flux (TSHF) averaged over the 100°–120°E zone for strong ENSO cases (El Niño − La Niña). TSHF is the sum of LH, SW, sensible heat flux (SF), and net downward longwave (LW) radiation. Contour intervals of LF, SW, and TSHF are all 5 W m^{-2}; positive (red) and negative (blue) anomalies of the SSTA, significant at the 95% level, are shaded. For LF, SW, and TSHF, downward flux that warms the ocean is defined as positive.

for the significant LF loss due to strengthened northeasterlies (Figs. 10a,b). According to Hartmann and Michelsen (1993), anomalies in the total surface heat flux (TSHF) over the tropical oceans are dominated by anomalies in LF and SW. Anomalies in TSHF into the ocean in the SSCS are negative after October(0) (Fig. 10c), which tends to maintain a negative SSTA there. Consequently, the warming in the SSCS cannot be explained by changes in the surface heat flux.

This observation contradicts Chen et al. (2007), who found that the surface heat flux is crucial in initiating the warming in SCS. A possible explanation for this difference may be that Chen et al. (2007) analyzed changes in the area-averaged surface heat flux over the central SCS (10°–20°N, 110°–120°E), whereas changes in surface heat flux over the central SCS are dominated by those over the NSCS (15°–20°N) during strong ENSO cases. Consequently, the fact that the warming in the SSCS cannot be explained by changes in the surface heat flux was not noted by Chen et al. (2007). We speculate that ocean dynamic processes, such as wind-induced advection and upwelling, may be responsible for the warming in the SSCS during El Niño events. Further study is required to verify this speculation and to provide a detailed understanding of the influence of various ocean dynamic processes on the SCS SSTA.

The central part of the southern low-level anomalous anticyclone (SLAAC) occurs at similar longitudes to those of the NLAAC in September(0); however, the SLAAC moves eastward more slowly than the NLAAC in October(0) and November(0). This is probably because the monsoon westerly over South Asia favors the transport of anticyclone anomalies toward the SCS and the Philippines in October(0) (Wang and Zhang 2002). The different movement speeds cause the central parts of the NLAAC and SLAAC to become aligned in a northeast–southwest direction. The SLAAC eventually anchors in the SEIO–northwest Australia regions and shows a gradual decay during the following winter and spring. The SLAAC induces southeasterly wind anomalies off Java and Sumatra in September(0) and October(0), which intensifies the prevailing southeasterlies in these regions. The strengthened southeasterlies result in increased surface evaporation (corresponding to enhanced LF loss), tending to cool the SEIO. Although the SLAAC suppresses the convection and increases the SW in the SEIO, it is unable to compensate for the LF loss due to strengthened southeasterlies (Fig. 10). In addition, the strengthened southeasterlies increase vertical mixing in the ocean and coastal upwelling (Shinoda et al. 2004; Kug and An 2010), intensifying the cooling in the SEIO. Therefore, the SEIO SSTA persistently cools in September(0) and October(0) in response to intensified southeasterlies, which may help to explain why the cooling is more intense in the SEIO than in the SCS during the period before the warming.

The southeasterlies in the SEIO begin to weaken after November(0) as the northeasterly winter monsoon flows gradually penetrate southward through the equator and become northwesterly flows in the Southern Hemisphere (Zhang and Zhang, 2010). The resulting decrease in LF loss, as well as the increased SW due to suppressed

convection, causes the SEIO SSTA to switch from negative to positive. In response to weakened southeasterlies in the SEIO, the upwelling along the coasts of Java and Sumatra also weakens, intensifying the warming in this region (Murtugudde et al. 2000).

The above analyses suggest that the sign reversal in the SCS and SEIO SSTA is closely related to the development and evolution of the NLAAC and SLAAC, respectively. Chen et al. (2007) reported that ENSO forces the NLAAC's eastward displacement via its accompanying large-scale divergence anomalies. However, ENSO-induced large-scale divergence anomalies are almost symmetrical in the north–south direction about the equator after October(0) (not shown), which is inconsistent with the asymmetry of the NLAAC that arises as it moves farther eastward than the SLAAC. The present results show that the seasonal cycle of the prevailing surface winds or trade winds plays an important role in the asymmetric eastward movements of the NLAAC and SLAAC.

The NLAAC and SLAAC form and develop in September(0) and October(0), which is the season of transition from the southwest summer monsoon to the northeast winter monsoon in the Northern Hemisphere. The northeasterly wind anomalies along the eastern flank of the NLAAC, which act to intensify the prevailing northeasterly monsoon flows, could involve a positive thermodynamic ocean–atmosphere feedback during the period after the NLAAC enters the Philippine Sea in winter (Wang et al. 2000). The NLAAC is sustained and trapped in the SCS–Philippines regions by the positive feedback until the ensuing spring, thereby maintaining cold SSTA to its east over the subtropical northwestern Pacific and warm SSTA to its west over the SCS. As the winter monsoon flows weaken, the NLAAC gradually decays during the following spring and summer.

In contrast, the SLAAC induces southeasterly wind anomalies to its east, weakening the prevailing cross-equatorial northwesterly flows over the SEIO and subtropical southwestern Pacific after December(0). In contrast to the NLAAC, the SLAAC is not driven by a positive thermodynamic ocean–atmosphere feedback. Consequently, the eastward extent of the SLAAC is confined to the Indian Ocean and it cannot move eastward to the subtropical southwestern Pacific. During the following spring and summer, the SSTA in the SEIO and subtropical southwestern Pacific shows a quicker decay than that in the SCS and subtropical northwestern Pacific.

By influencing the eastward extent of the NLAAC and SLAAC associated with ENSO, the seasonal cycle of the prevailing surface winds determines the times when the SCS FPB and the SEIO WPB occur. The SCS FPB occurs in fall, which is the season of transition from the southwest summer monsoon to the northeast winter monsoon in the Northern Hemisphere, while the SEIO WPB occurs in winter, which is the season of transition from prevailing southeasterly flows to prevailing cross-equatorial northwesterly flows over the SEIO. The WIO SPB occurs in spring, which is also consistent with the season of transition from winter monsoon flows to summer monsoon flows over the WIO.

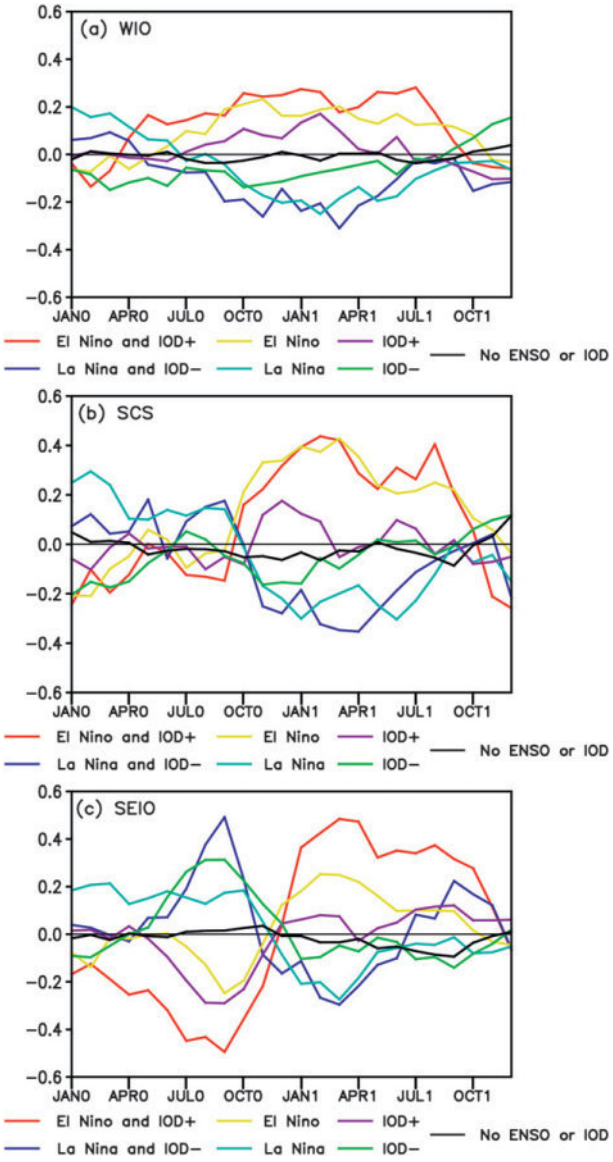

FIG. 11. Composite difference of the area-averaged SSTA (°C) over the (a) WIO, (b) SCS, and (c) SEIO for categories of the ENSO–IOD relationship listed in Table 2.

6. Influences of IOD on the persistence of the TIO SSTA

Figures 11a–c show the composite difference of the area-averaged SSTA over the WIO, SCS, and SEIO,

respectively, for the categories of the ENSO–IOD relationship listed in Table 2. The evolution of the WIO SSTA for El Niño with positive IOD (or La Niña with negative IOD) is similar to that for pure El Niño (or pure La Niña) (Fig. 11a). For these categories, the WIO SSTA shows a slight reversal in sign from negative to positive (or from positive to negative) during spring. It then slowly increases (or decreases) and reaches a peak in the spring of the following year. The WIO SSTA for pure positive IOD (or pure negative IOD) does not show a reversal in sign during spring, and it does not show a significant warming (or cooling) trend in the ensuing summer and winter, for both categories. The composites of the WIO SSTA for no-ENSO or IOD show a very small amplitude. Consistent with the evolution of the WIO SSTA, the persistence analyses for different ENSO/IOD categories show that a weak SPB only exists in the WIO SSTA in the case that ENSO co-occurs with IOD and pure ENSO (not shown). The WIO SPB is absent during pure IOD and neutral (no-ENSO or IOD) years. These results indicate that the WIO SPB is caused mainly by ENSO rather than by IOD.

The SCS SSTA shows a rapid reversal in sign, mainly during fall, when El Niño (or La Niña) occurs with or without positive IOD (or negative IOD) (Fig. 11b). After the reversal, it shows a rapid warming or cooling and persists for several months until the following summer in these categories. The amplitude of the SCS SSTA is relatively small for both pure positive IOD and pure negative IOD, and it shows a slow minor increase during winter in both categories, followed by a rapid decay in early spring. The reversal in sign of the SCS SSTA is less distinct for pure IOD events. The amplitude of the SCS SSTA for no-ENSO or IOD is very small, and its evolution is relatively irregular. Corresponding to the rapid sign reversal of the SCS SSTA during fall, a well-defined FPB is found during ENSO co-occurring with IOD and pure ENSO (not shown). The SCS SPB is indistinct during pure IOD and neutral (no-ENSO or IOD) years. These results suggest that the SCS FPB is dependent mainly on ENSO and is relatively independent of IOD, similarly to the WIO SPB.

The SEIO SSTA shows an evident quasi-biennial oscillation when El Niño or La Niña occurs with an IOD event (Fig. 11c). The amplitude of the oscillation is significantly greater for El Niño with a positive IOD than for La Niña with a negative IOD, possibly because of the asymmetry of ENSO and the IOD (An and Jin 2004; Hong et al. 2008a,b; Su et al. 2010). As noted in previous studies (Hong et al. 2010; Wu et al. 2010), the asymmetry of ENSO and the IOD can lead to the asymmetry of atmospheric and oceanic response to the opposite phases of ENSO forcing. Hong et al. (2010) reported that the amplitude asymmetry between the basinwide warming and cooling in the Indian Ocean appears only when ENSO is concurrent with IOD, and it becomes insignificant during pure ENSO and pure IOD events. Figure 11c shows that the amplitude asymmetry of the SEIO SSTA is only significant during the combined ENSO–IOD events, consistent with the findings of Hong et al. (2010).

The phase reversal of the SEIO SSTA occurs mainly during winter in cases where ENSO co-occurs with IOD, or during a pure ENSO event. Because of the amplitude asymmetry, the sign reversal of the SEIO SSTA in winter is stronger for El Niño with a positive IOD than during either La Niña with a negative IOD or pure ENSO years. According to the above analysis, the strengths of the persistence barriers are generally consistent with those of the SSTA sign reversal. The strongest sign reversal of the SEIO SSTA may lead to the strongest SEIO WPB during El Niño with a positive IOD. However, because autocorrelation calculated using only small amounts of data (only seven combined El Niño–positive IOD events in Table 2) become unreliable, we do not show a comparison of the SSTA persistence between El Niño with a positive IOD and La Niña with a negative IOD. Instead, we show the persistence analyses of the SEIO SSTA for ENSO co-occurring with IOD, and for a pure ENSO event. The results show a prominent WPB in the SEIO for ENSO co-occurring with IOD and for pure ENSO (Fig. 12). The SEIO WPB during ENSO co-occurring with IOD is slightly more prominent than that during pure ENSO. We suggest that the strengthened SEIO WPB when ENSO co-occurs with IOD is mainly caused by the asymmetry of the SEIO SSTA driven by the ENSO remote forcing.

The SEIO SSTA for pure positive IOD and pure negative IOD also undergoes a sign reversal during winter, but the reversal is relatively weak due to the rapid decay of the SSTA after winter. The amplitude of the SEIO SSTA is very small, and no phase reversal of SSTA occurs in no-ENSO or IOD cases. The persistence analyses show that when pure IOD events occur, the SEIO WPB is also found, but is weaker than that for ENSO co-occurring with IOD or a pure ENSO event (Fig. 12). The SEIO WPB is indistinct during no-ENSO or IOD years.

These results clearly demonstrate that in addition to ENSO, IOD alone can cause a weak WPB in the SEIO SSTA. El Niño events co-occurring with positive IOD act to further strengthen the SEIO WPB, leading to the most prominent WPB. It therefore appears that the SEIO WPB is influenced more by ENSO than by IOD. This conclusion differs from the findings of Wajsowicz (2005), who emphasized the influence of IOD (rather than ENSO) on the SEIO WPB.

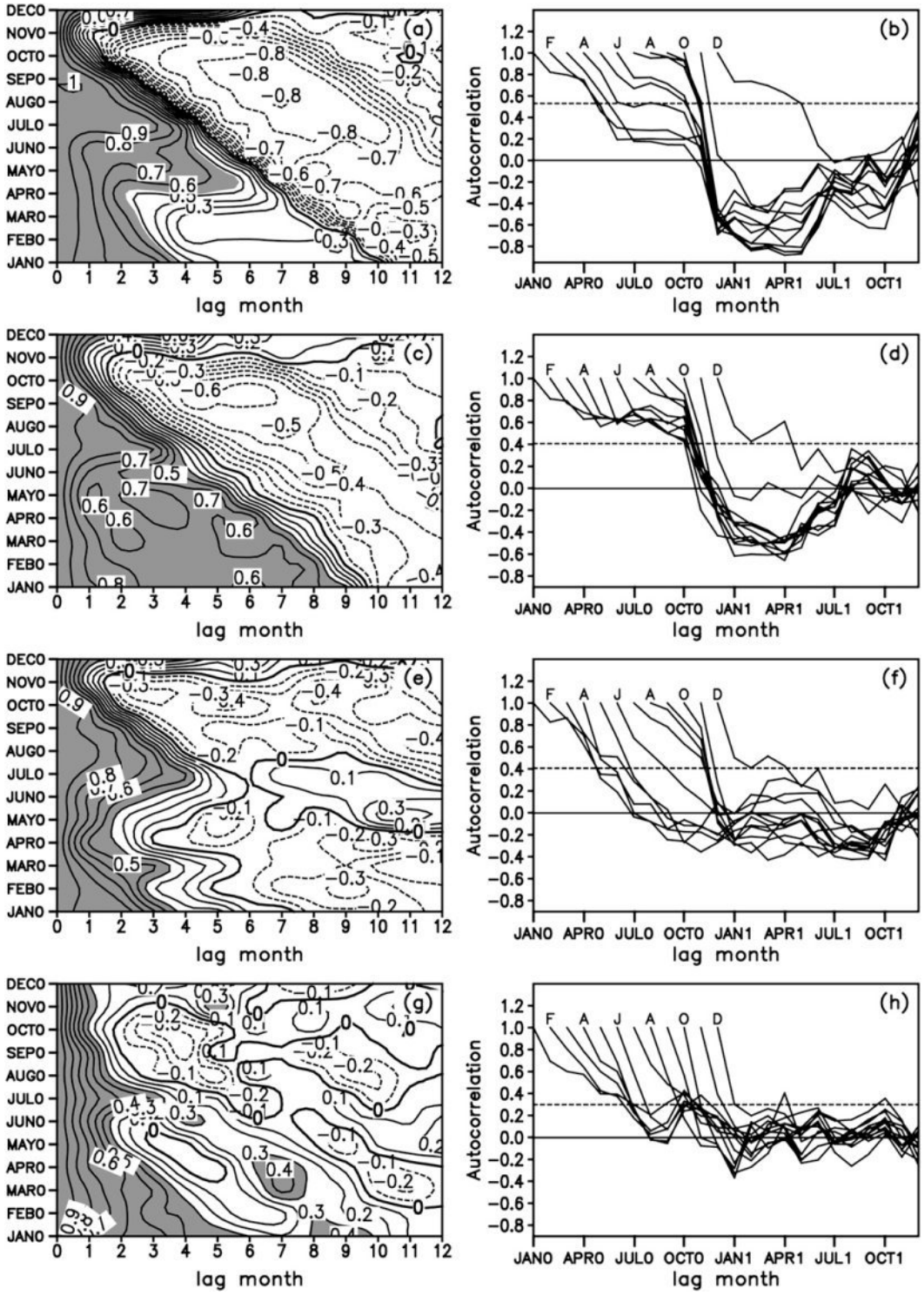

FIG. 12. (left) Autocorrelations of the area-averaged SSTA over the SEIO as a function of starting calendar month and lag time for (a) El Niño with positive IOD and La Niña with negative IOD, (c) pure El Niño and pure La Niña, (e) pure positive IOD and pure negative IOD, and (g) no-ENSO or IOD. (right) Autocorrelation curves of the WIO as a function of starting calendar month and lag time for (b) El Niño with positive IOD and La Niña with negative IOD, (d) pure El Niño and pure La Niña, (f) pure positive IOD and pure negative IOD, and (h) no-ENSO or IOD. In (a),(c),(e), and (g), the zero contour is highlighted; autocorrelations significant at the 95% level are shaded. In (b),(d),(f), and (h), the horizontal dashed line indicates the 95% significance level.

On monthly scales, both the ENSO and IOD have significant impacts on the SEIO SSTA. However, it is important to examine why ENSO alone produces a prominent WPB in the SEIO SSTA, whereas IOD alone only produces a weak WPB. One possible reason for this difference is that the ENSO influence on the SEIO SSTA persists for longer than the IOD influence. The IOD events develop in summer and attain a peak in fall, followed by a rapid decay in winter (Saji et al. 1999); consequently, the influence of IOD on the SEIO SSTA is mainly limited to summer and fall. When pure IOD events occur, the SEIO SST shows a relatively large anomaly in summer and fall, but a small anomaly in the following winter and spring. The quasi-biennial oscillation of the SEIO SSTA becomes indistinct for pure IOD events; consequently, the SEIO SSTA shows only a slight sign reversal in winter associated with pure IOD events, ultimately resulting in a weak WPB. In contrast, the influence of ENSO on the SEIO SSTA is present throughout the ensuing winter and spring. When pure ENSO events occur, the SEIO SST shows a relatively large anomaly in summer and fall, and a large anomaly of the opposite sign during the following winter and spring. The quasi-biennial oscillation of the SEIO SSTA is prominent for pure ENSO events. Consistent with this observation, the SEIO SSTA shows a strong sign reversal in winter, ultimately resulting in a strong WPB.

Clarke and Van Gorder (1999) reported that the biennial oscillation embedded in the ENSO index might be responsible for the prominent SPB in the eastern equatorial Pacific, which is phase-locked to the calendar year. We speculate that the quasi-biennial signal of the SEIO SSTA, which is closely linked to ENSO, might play an important role in the occurrence of the SEIO WPB. Nicholls (1984) also postulated that the SEIO WPB is related to a biennial cycle, and this cycle is probably driven by variations in air–sea interaction through the year caused by the seasonal reversal of the zonal winds in this region. Although the quasi-biennial signal of the SCS SSTA associated with ENSO is not as prominent as that of the SEIO SSTA, it does exist in the SCS SSTA, producing a well-defined FPB. Further research is necessary to examine the dynamic relationships among the persistence barriers, ENSO, and the quasi-biennial oscillation, and to consider the implications of these relationships in terms of improving predictions of the TIO SSTA.

7. Summary

This study aimed to investigate the persistence characteristics of the SST anomaly (SSTA) in the tropical Indian Ocean (TIO) that is associated with ENSO. Since the persistence of the SSTA is closely linked to its monthly evolution, we first examined in detail the evolutionary features of the ENSO-induced TIO SSTA. During El Niño cases, a sign reversal of SSTA, from negative to positive, occurs successively in the western TIO (10°S–10°N, 50°–70°E) during spring, in the South China Sea (5°–20°N, 100°–120°E) during fall, and in the southeastern TIO (15°S–0°, 100°–120°E) during winter (Fig. 13). The intensity of this sign reversal varies in different TIO subdomains, with a less abrupt reversal in the western TIO, an abrupt reversal in the South China Sea, and the most abrupt reversal in the southeastern TIO.

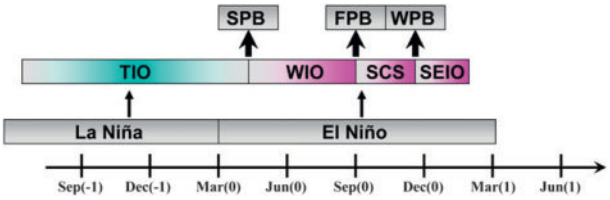

FIG. 13. Seasonality of sign reversals and persistence barriers of the ENSO-induced TIO SSTA. Pink (blue) shading indicates anomalous warming (cooling) induced by ENSO. Black arrows indicate the occurrence times of SSTA sign reversals and persistence barriers in the WIO, SCS, and SEIO.

The SSTA sign reversals that occur in the western TIO, South China Sea, and southeastern TIO may reduce the persistence of the anomaly, creating favorable conditions for the occurrence of the persistence barrier. Autocorrelation analyses of area-averaged SSTA over the western TIO, South China Sea, and southeastern TIO show a weak spring persistence barrier (SPB) in the western TIO, a strong fall persistence barrier (FPB) in the South China Sea, and the strongest winter persistence barrier (WPB) in the southeastern TIO (Fig. 13). The occurrence seasons and strengths of the persistence barriers are consistent with those of the SSTA sign reversal, indicating a close connection between the two phenomena. The sign reversal of the SSTA in the western TIO, South China Sea, and southeastern TIO shows a weakening in intensity during weak ENSO cases, and does not occur during normal cases. As a result, the barriers in the western TIO, South China Sea, and southeastern TIO become indiscernible or disappear in these cases.

The schematic in Fig. 14 summarizes a possible explanation of processes by which ENSO successively causes a sign reversal in the western TIO, South China Sea, and southeastern TIO SSTA. In winter and early spring before an El Niño event occurs, negative SSTA dominates the TIO, possibly caused by La Niña preceded by El Niño. As the La Niña event enters its decaying phase in spring, the negative SSTA in the western TIO gradually

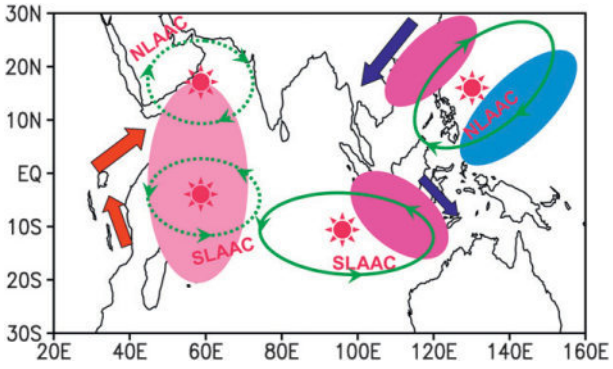

FIG. 14. Schematic diagram summarizing the processes that may explain how ENSO causes successive sign reversals in the WIO, SCS, and SEIO SSTA. NLAAC and SLAAC indicate the northern and southern low-level anomalous anticyclones, respectively. Dashed ovals with arrowheads indicate the approximate initial position of the NLAAC and SLAAC during September(0), and solid ovals with arrowheads indicate the approximate final position of the NLAAC and SLAAC after December(0). Red suns in the middle of the NLAAC and SLAAC indicate enhanced net shortwave downward radiation around these regions. Pink shading indicates the anomalous warming induced by the NLAAC/SLAAC during October(0), while magenta (blue) shading indicates the anomalous warming (cooling) induced by the NLAAC/SLAAC after December(0). Red and blue arrows indicate the prevailing surface winds during September(0) and December(0), respectively.

evolves to a positive, and the western TIO SSTA experiences a slow sign reversal from negative to positive. In September(0), when El Niño enters its developing stage, El Niño–induced changes in the Walker circulation produce a pair of low-level anticyclonic anomalies on each side of the equator (Gill 1980; Wang and Zhang 2002), with their centers located around the Arabian Sea and the southwestern TIO. The two anticyclonic anomalies induce an antisymmetric wind pattern that weakens the prevailing surface winds and causes the western TIO SSTA to warm significantly in October(0). The two anticyclonic anomalies intensify quickly and move eastward in October(0) and November(0). The northern low-level anomalous anticyclone (NLAAC) moves farther eastward into the western North Pacific, with its center over the Philippines in December(0) (Wang et al. 2000; Wang and Zhang 2002). The eastward passage of the NLAAC across the South China Sea induces a rapid warming in the northern South China Sea via weakening of the prevailing northeasterlies and suppressed convection in the region (Chen et al. 2007). Consequently, the South China Sea SST shows a rapid change from a negative to a positive anomaly during fall.

The southern low-level anomalous anticyclone (SLAAC) moves eastward more slowly than the NLAAC in October(0) and November(0), and eventually anchors in the southeastern TIO–northwest Australia regions during the following winter and spring. The SLAAC induces southeasterly wind anomalies off Java and Sumatra in September(0) and October(0), resulting in enhanced prevailing southeasterlies and a cooler SST in the region. However, as the northeasterly winter monsoon flows gradually penetrate southward across the equator after December(0) (Zhang and Zhang, 2010), the prevailing cross-equatorial northwesterly flows off Java and Sumatra are weakened by the southeasterly wind anomalies induced by the SLAAC. The decrease in the latent heat flux (LF) loss caused by lower wind speeds, combined with the increased net downward shortwave (SW) radiation due to suppressed convection, causes the southeastern TIO SSTA to switch from negative to positive. In addition, the weakened southeasterlies decrease vertical mixing in the ocean and coastal upwelling, intensifying the warming in the SEIO (Murtugudde et al. 2000). Consequently, the southeastern TIO SSTA shows an abrupt change from negative to positive during winter.

The persistence barrier of the western TIO SSTA is locked to spring, while the barriers of the South China Sea and southeastern TIO SSTA are locked to fall and winter, respectively. The present results show that the seasonal cycle of the prevailing surface winds has an important influence on the timing of the persistence barriers in the TIO. The western TIO SPB occurs in spring, which is consistent with the season of transition from winter monsoon flows to summer monsoon flows over the western TIO. The South China Sea FPB occurs in fall, which is the season of transition from the southwest summer monsoon to the northeast winter monsoon in the Northern Hemisphere, while the southeastern TIO WPB occurs in winter, which is the season of transition from prevailing southeasterly flows to prevailing cross-equatorial northwesterly flows over the southeastern TIO.

In addition to ENSO, the Indian Ocean dipole (IOD) modulates the evolution of the SSTA in the TIO, thereby affecting the SSTA persistence in this region. The present results show that the IOD alone can cause a weak WPB in the southeastern TIO SSTA. El Niño events co-occurring with positive IOD act to further strengthen the southeastern TIO WPB, leading to the most prominent WPB. It appears that the southeastern TIO WPB is influenced more strongly by ENSO than by the IOD. In contrast, the western TIO SPB and the South China Sea FPB are strongly dependent on ENSO and are relatively independent of the IOD.

Acknowledgments. We wish to thank three anonymous reviewers for their constructive comments and suggestions, which helped to substantially improve the quality

of this paper. This research was funded by the 973 program (2010CB950400) and an NSFC Project (41175069).

REFERENCES

Alexander, M. A., I. Bladé, M. Newman, J. R. Lanzante, N.-C. Lau, and J. D. Scott, 2002: The atmospheric bridge: The influence of ENSO teleconnections on air–sea interaction over the global oceans. *J. Climate,* **15,** 2205–2231.

Alory, G., S. Wijffels, and G. Meyers, 2007: Observed temperature trends in the Indian Ocean over 1960–1999 and associated mechanisms. *Geophys. Res. Lett.,* **34,** L02606, doi:10.1029/2006GL028044.

An, S.-I., and F.-F. Jin, 2004: Nonlinearity and asymmetry of ENSO. *J. Climate,* **17,** 2399–2412.

Ashok, K., W.-L. Chan, T. Motoi, and T. Yamagata, 2004: Decadal variability of the Indian Ocean dipole. *Geophys. Res. Lett.,* **31,** L24207, doi:10.1029/2004GL021345.

Chen, J.-M., L. Tim, and C.-F. Shih, 2007: Fall persistence barrier of sea surface temperature in the South China Sea associated with ENSO. *J. Climate,* **20,** 158–172.

Chowdary, J. S., and C. Gnanaseelan, 2007: Basin-wide warming of the Indian Ocean during El Niño and Indian Ocean dipole years. *Int. J. Climatol.,* **27,** 1421–1438.

Clarke, A. J., and S. Van Gorder, 1999: The connection between the boreal spring Southern Oscillation persistence barrier and biennial variability. *J. Climate,* **12,** 610–620.

Ding, R.-Q., and J.-P. Li, 2009: Decadal and seasonal dependence of North Pacific SST persistence. *J. Geophys. Res.,* **114,** D01105, doi:10.1029/2008JD010723.

——, and ——, 2011: Winter persistence barrier of sea surface temperature in the northern tropical Atlantic associated with ENSO. *J. Climate,* **24,** 2285–2299.

——, K.-J. Ha, and J.-P. Li, 2009: Interdecadal shift in the relationship between the East Asian summer monsoon and the tropical Indian Ocean. *Climate Dyn.,* **34,** 1059–1071.

Du, Y., S.-P. Xie, G. Huang, and K.-M. Hu, 2009: Role of air–sea interaction in the long persistence of El Niño–induced north Indian Ocean warming. *J. Climate,* **22,** 2023–2038.

Duan, W., X. Liu, K. Zhu, and M. Mu, 2009: Exploring initial errors that cause a significant "spring predictability barrier" for El Niño events. *J. Geophys. Res.,* **114,** C04022, doi:10.1029/2008JC004925.

Enfield, D. B., 1996: Relationships of inter-American rainfall to tropical Atlantic and Pacific SST variability. *Geophys. Res. Lett.,* **23,** 3305–3308.

——, and D. A. Mayer, 1997: Tropical Atlantic sea surface temperature variability and its relation to El Niño–Southern Oscillation. *J. Geophys. Res.,* **102** (C1), 929–945.

Giannini, A., J. C. H. Chiang, M. A. Cane, Y. Kushnir, and R. Seager, 2001: The ENSO teleconnection to the tropical Atlantic Ocean: Contributions of the remote and local SSTs to rainfall variability in the tropical Americas. *J. Climate,* **14,** 4530–4544.

Gill, A. E., 1980: Some simple resolutions for heat-induced tropical circulation. *Quart. J. Roy. Meteor. Soc.,* **106,** 447–462.

Goswami, B. N., and J. Shukla, 1991: Predictability of a coupled ocean–atmosphere model. *J. Climate,* **4,** 3–22.

Hartmann, D. L., and M. L. Michelsen, 1993: Large-scale effects on the regulation of tropical sea surface temperature. *J. Climate,* **6,** 2049–2062.

Hong, C. -C., T. Li, J.-S. LinHo, and J.-S. Kug, 2008a: Asymmetry of Indian Ocean dipole. Part I: Observational analysis. *J. Climate,* **21,** 4834–4848.

——, ——, and J.-J. Luo, 2008b: Asymmetry of Indian Ocean dipole. Part II: Model diagnosis. *J. Climate,* **21,** 4849–4858.

——, ——, Y.-C. LinHo, and Y.-C. Chen, 2010: Asymmetry of the Indian Ocean basinwide SST anomalies: Roles of ENSO and IOD. *J. Climate,* **23,** 3563–3576.

Kalnay, E., and Coauthors, 1996: The NCEP–NCAR 40-Year Reanalysis Project. *Bull. Amer. Meteor. Soc.,* **77,** 437–471.

Kawamura, R., T. Matsumura, and S. Iizuka, 2001: Role of equatorially asymmetric sea surface temperature anomalies in the Indian Ocean in the Asian summer monsoon and El Niño–Southern Oscillation coupling. *J. Geophys. Res.,* **106** (D5), 4681–4693.

Klein, S. A., B. J. Soden, and N.-C. Lau, 1999: Remote sea surface temperature variations during ENSO: Evidence for a tropical atmospheric bridge. *J. Climate,* **12,** 917–932.

Kug, J.-S., and S.-I. An, 2010: Ocean dynamic processes responsible for the interannual variability of the tropical Indian Ocean SST associated with ENSO. *Atmosphere,* **20,** 211–219.

Lau, N.-C., and M. J. Nath, 2003: Atmosphere–ocean variations in the Indo-Pacific sector during ENSO episodes. *J. Climate,* **16,** 3–20.

Luo, J.-J., S. Masson, S. Behera, and T. Yamagata, 2007: Experimental forecasts of Indian Ocean dipole using a coupled OAGCM. *J. Climate,* **20,** 2178–2190.

Meyers, G., P. McIntosh, L. Pigot, and M. Pook, 2007: The years of El Niño, La Niña, and interactions with the tropical Indian Ocean. *J. Climate,* **20,** 2872–2880.

Murtugudde, R., J. P. McCreary, and A. J. Busalacchi, 2000: Oceanic processes associated with anomalous events in the Indian Ocean with relevance to 1997–1998. *J. Geophys. Res.,* **105** (C2), 3295–3306.

Nicholls, N., 1984: The Southern Oscillation and Indonesian sea surface temperature. *Mon. Wea. Rev.,* **112,** 424–432.

Nobre, P., and J. Shukla, 1996: Variations of sea surface temperature, wind stress, and rainfall over the tropical Atlantic and South America. *J. Climate,* **9,** 2464–2479.

Rasmusson, E. M., X. Wand, and C. F. Ropelewski, 1990: The biennial component of ENSO variability. *J. Mar. Syst.,* **1,** 71–96.

Rayner, N. A., P. Brohan, D. E. Parker, C. K. Folland, J. J. Kennedy, M. Vanicek, T. Ansell, and S. F. B. Tett, 2006: Improved analyses of changes and uncertainties in sea surface temperature measured in situ since the mid-nineteenth century: The HadSST2 dataset. *J. Climate,* **19,** 446–469.

Saji, N. H., B. N. Goswami, P. N. Vinayachandran, and T. Yamagata, 1999: A dipole mode in the tropical Indian Ocean. *Nature,* **401,** 360–363.

Schott, F. A., S.-P. Xie, and J. P. McCreary Jr., 2009: Indian Ocean circulation and climate variability. *Rev. Geophys.,* **47,** RG1002, doi:10.1029/2007RG000245.

Shinoda, T., M. A. Alexander, and H. H. Hendon, 2004: Remote response of the Indian Ocean to interannual SST variations in the tropical Pacific. *J. Climate,* **17,** 362–372.

Su, J.-Z., R.-H. Zhang, T. Li, X.-Y. Rong, J.-S. Kug, and C.–C. Hong, 2010: Causes of the El Niño and La Niña amplitude asymmetry in the equatorial eastern Pacific. *J. Climate,* **23,** 605–617.

Tokinaga, H., and Y. Tanimoto, 2004: Seasonal transition of SST anomalies in the tropical Indian Ocean during El Niño and Indian Ocean dipole years. *J. Meteor. Soc. Japan,* **82,** 1007–1018.

Torrence, C., and P. J. Webster, 1998: The annual cycle of persistence in the El Niño–Southern Oscillation. *Quart. J. Roy. Meteor. Soc.,* **124,** 1985–2004.

Venzke, S., M. Latif, and A. Villwock, 2000: The coupled GCM ECHO-2. Part II: Indian Ocean response to ENSO. *J. Climate,* **13,** 1317–1383.

Wajsowicz, R. C., 2005: Potential predictability of tropical Indian Ocean SST anomalies. *Geophys. Res. Lett.,* **32,** L24702, doi:10.1029/2005GL024169.

Wang, B., and Q. Zhang, 2002: Pacific–East Asian teleconnection. Part II: How the Philippine Sea anomalous anticyclone is established during El Niño development. *J. Climate,* **15,** 3252–3265.

——, R. Wu, and X. Fu, 2000: Pacific–East Asian teleconnection: How does ENSO affect East Asian climate. *J. Climate,* **13,** 1517–1536.

Webster, P. J., and S. Yang, 1992: Monsoon and ENSO: Selectively interactive systems. *Quart. J. Roy. Meteor. Soc.,* **118,** 877–925.

Wu, B., T. Li, and T.-J. Zhou, 2010: Asymmetry of atmospheric circulation anomalies over the western North Pacific between El Niño and La Niña. *J. Climate,* **23,** 4807–4822.

Xie, S.-P., H. Annamalai, F. Schott, and J. P. McCreary Jr., 2002: Origin and predictability of South Indian Ocean climate variability. *J. Climate,* **15,** 864–878.

——, K.-M. Hu, J. Hafner, Y. Du, G. Huang, and H. Tokinaga, 2009: Indian Ocean capacitor effect on Indo-western Pacific climate during the summer following El Niño. *J. Climate,* **22,** 730–747.

Yu, J.-Y., 2005: Enhancement of ENSO's persistence barrier by biennial variability in a coupled atmosphere–ocean general circulation model. *J. Geophys. Res.,* **32,** L13707, doi:10.1029/2005GL023406.

Zebiak, S. E., and M. A. Cane, 1987: A model El Niño–Southern Oscillation. *Mon. Wea. Rev.,* **115,** 2262–2278.

Zhang, C.-J., and H.-Q. Zhang, 2010: Potential impacts of East Asian winter monsoon on climate variability and predictability in the Australian summer monsoon region. *Theor. Appl. Climatol.,* **101,** 161–177.

Zhao, X., and J.-P. Li, 2009: Possible causes for the persistence barrier of SSTA in the South China Sea and the vicinity of Indonesia. *Adv. Atmos. Sci.,* **26,** 1125–1136.